

Gain characterization of LGAD sensors with beta particles and 28-MeV protons

M. H. Mohamed Farook,^a G. Giacomini,^c G. D'Amen,^b G. Pinaroli,^c E. Rossi,^c S. Seidel,^a and A. Tricoli^{b,1}

^a*Department of Physics and Astronomy, University of New Mexico, Albuquerque, New Mexico, USA*

^b*Physics Department, Brookhaven National Laboratory, Upton, New York, USA*

^c*Instrumentation Department, Brookhaven National Laboratory, Upton, New York, USA*

E-mail: atricoli@bnl.gov

ABSTRACT: Low Gain Avalanche Diodes, also known as LGADs, are widely considered for fast-timing applications in high energy physics, nuclear physics, space science, medical imaging, and precision measurements of rare processes. Such devices are silicon-based and feature an intrinsic gain due to a p^+ -doped layer that allows the production of a controlled avalanche of carriers, with multiplication on the order of 10-100. This technology can provide time resolution on the order of 20-30 ps, and variants of this technology can provide precision tracking too. The characterization of LGAD performance has so far primarily been focused on the interaction of minimum ionizing particles for high energy and nuclear physics applications. This article expands the study of LGAD performance to highly-ionizing particles, such as 28-MeV protons, which are relevant for several future scientific applications, e.g. in biology and medical physics, among others. These studies were performed with a beam of 28-MeV protons from a tandem Van de Graaff accelerator at Brookhaven National Laboratory and beta particles from a ^{90}Sr source; these were used to characterize the response and the gain of an LGAD as a function of bias voltage and collected charge. The experimental results are also compared to TCAD simulations.

KEYWORDS: Solid state detectors, Particle tracking detectors, Timing detectors, protons, electrons

¹Corresponding author.

Contents

1	Introduction	1
2	Experimental apparatus	2
3	Particle beams and data selection	3
3.1	Beta ^{90}Sr source	3
3.2	28-MeV proton beam	4
3.3	Signal pulses in data	5
4	Signal properties	5
4.1	Signal properties in diodes	6
4.2	Signal properties in LGADs	6
5	Gain Measurements	7
5.1	Gain from signal amplitudes	8
5.1.1	Gain with 28-MeV protons	9
5.1.2	Gain with beta-particles	9
5.2	Gain from collected charge	11
5.2.1	Gain with 28-MeV protons	11
5.2.2	Gain with beta particles	12
6	Simulation	12
7	Comparison of results	14
8	Conclusions	17
A	Measurement of the number of electron-hole pairs generated by a MIP in silicon	17
B	Measurement of the Amplifier Gain	17

1 Introduction

Fast-timing detectors have attracted widespread interest for their applications to the development of the next generation of colliders in high energy physics experiments and for other applications including nuclear physics, space science, medical imaging, and precision measurements of rare processes. In this context, silicon-based particle sensors with fast-timing capabilities on the order of 30 ps are a rapidly developing research area, for application in timing systems for the upgraded ATLAS and CMS experiments [1, 2] at the CERN Large Hadron Collider (LHC) for the High

Luminosity phase (HL-LHC) [3, 4]. One of the selected technologies for such detectors is a silicon pad with internal amplification, i.e. the Low Gain Avalanche Diode (LGAD) [5–7]. The principle of operation of an LGAD is based on the creation of a thin layer of high electric field at the n^{++} and p^+ junction where the signal is amplified by avalanche multiplication to achieve a gain of about 10-100. The LGADs for the HL-LHC are implemented as a 50 μm thick p -type bulk silicon sensor with a highly doped p^+ layer, called the gain layer, under the n^{++} electrode. Such sensors have also been fabricated recently on a thinner p -type active substrate, e.g. 20, 30, 33, 35 or 45 μm , to achieve faster time performance [8–12]. Variants of the LGAD technology, e.g. the AC-coupled LGADs (AC-LGADs) [13, 14], have been proposed for four-dimensional detectors in nuclear physics experiments, such as the ePIC experiment at the Electron-Ion Collider (EIC) [15], since they provide time resolution similar to that of LGADs and segmentation as small as a few tens of microns with a fill factor of 100%. While this article focuses on the LGAD performance, the general features of the results are expected to hold also in the case of AC-LGADs.

So far, the characterization of LGAD performance has focused primarily on the interaction of minimum ionizing particles (MIPs) for high energy physics and nuclear physics applications. This article expands the study to highly-ionizing particles (non-MIPs), which are relevant for future scientific applications in biology, medical physics, and precision measurements of rare processes, where low energy protons, pions, kaons or heavy ions are used. Among such applications, it is worth highlighting those in micro-dosimetry for radiotherapy, where low energy protons (≤ 200 MeV beam energy) are used as well as heavy-ion beams such as carbon [16]. Also relevant is the PIONEER experiment at PSI [17], where low energy electrons and muons are detected to measure the ratios of the decay rates of charged pions to prompt electrons and muons.

While MIPs produce about 60-80 electron-hole pairs per micron in thin silicon sensors, non-MIPs can produce a far greater amount of charge in silicon, and this may affect the signal properties of LGADs due to different charge multiplication and collection processes. This article reports the study of LGAD signal properties performed with a beam of 28-MeV protons (which are non-MIP) from a tandem Van de Graaff accelerator at Brookhaven National Laboratory [18]. The results are compared to those obtained with a beam of beta particles (MIPs) from a ${}^{90}\text{Sr}$ source and to TCAD simulations to facilitate their interpretation. The gain and other properties of an LGAD are measured as a function of bias voltage and compared to those of diodes, i.e. sensors designed and fabricated with the same process and geometry as the LGAD but without the p^+ -doped gain layer.

2 Experimental apparatus

Three silicon sensors were used for this study. They were fabricated by Hamamatsu Photonics (HPK): one LGAD of HPK type 3.1 [19], and two diodes (Diode-1 and Diode-2). Two diodes were used for systematic checks. All the sensors are single-pad of size $1.3 \times 1.3 \text{ mm}^2$ and active thickness 35 μm . Figure 1 (top) shows one diode and the LGAD. The LGAD is fully depleted at about 35 V. At operating bias voltage ≥ 100 V the detector capacitance is about 5.5 pF. The LGAD current starts to go into the breakdown region at a bias voltage of about 250 V, and at bias voltages in the range 100 – 250 V the leakage current is approximately 4.7 – 7.1 nA.

The three sensors were mounted on the same readout board, which was designed by FNAL, see Figure 1 (bottom). It is a 16-channel board with two-stage amplification based on the Mini-

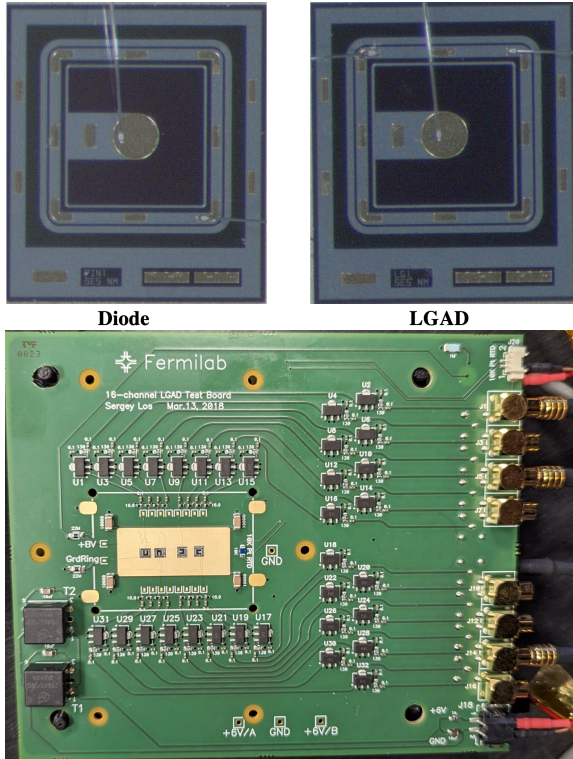


Figure 1: A diode (top-left) and the LGAD (top-right) sensors fabricated by HPK. The photos also shows the wire-bonds connected to the pads and the guard-rings. The FNAL readout board (bottom) is shown with sensors mounted and wire-bonded. (One additional sensor is mounted on the board, but it was found not to be well functioning and was not used for this study.)

Circuits GALI-66+ integrated circuit [20]. The amplifiers use $50\ \Omega$ input impedance, for a total transimpedance of approximately $5\text{ k}\Omega$ and a bandwidth of 3 GHz [19].

The diode and LGAD pulses were recorded using a four-channel Lecroy Waverunner 9404M-MS oscilloscope with a bandwidth of 1 GHz and a sampling rate of 10 GS/s per channel.

3 Particle beams and data selection

To characterize the performance of the sensors with non-MIPs, a beam of 28-MeV protons was used. Beta particles from a ^{90}Sr radioactive source were used for MIP interactions. The stopping power of a 28-MeV proton is $15.5\text{ MeV cm}^2/\text{g}$. For reference, that for a 2.25-GeV proton (a MIP) is $1.7\text{ MeV cm}^2/\text{g}$, which is numerically very close to the stopping power of a 2.28-MeV beta-particle from the decay chain of a ^{90}Sr radioactive source, which is $1.6\text{ MeV cm}^2/\text{g}$ [21]. Therefore, the energy deposited in silicon by a 28-MeV proton is one order of magnitude greater than that of a MIP.

3.1 Beta ^{90}Sr source

The ^{90}Sr radioactive source was used with a 1 mm thick aluminum layer placed in front to absorb low energy beta particles and select the 2.28-MeV ones from the decay chain. The radioactive source,

placed about a centimeter from the device under test, illuminated the junction side of the devices. The entire setup was enclosed in a metallic light-proof box for electromagnetic shielding. The measurements were taken at room temperature. The lowest trigger level used for the oscilloscope to record events was 8 mV. Events recorded by the oscilloscope were rejected if they were compatible with pick-up noise in the readout electronics.

The ^{90}Sr radioactive source was not used for the diodes because the signals are very small and the triggering threshold, after tuning to reject the noise, cut the peak of the amplitude spectrum.

3.2 28-MeV proton beam

The tandem Van de Graaff Facility at BNL consists of two 15-MV electrostatic accelerators capable of delivering continuous or high-intensity pulsed ion beams to experimental chambers in a wide range of ion species at various energies [18]. For this experiment a beam of 28-MeV protons was used with a flux in the range $1\text{-}5 \times 10^4$ protons/(s cm 2). Data were recorded for between 5 minutes and 40 minutes per working point. At least 10,000 events were collected for diodes and for the LGAD at bias voltages below 200 V, and at least 80,000 events were collected for the LGAD at higher voltages. The FNAL readout board with the sensors was placed inside a vacuum chamber that is located at the end of the beam line. The board was connected through a thermal glue to a cold chuck that kept the temperatures stable at about 25°C using a chiller that ran with a fluid consisting of a mix of water and glycol. High voltage to the devices under test was provided by a 16-channel CAEN multi-channel power supply unit which was placed outside the vacuum chamber and controlled remotely by the operators in a control-room through a custom-made interface based on Python drivers.

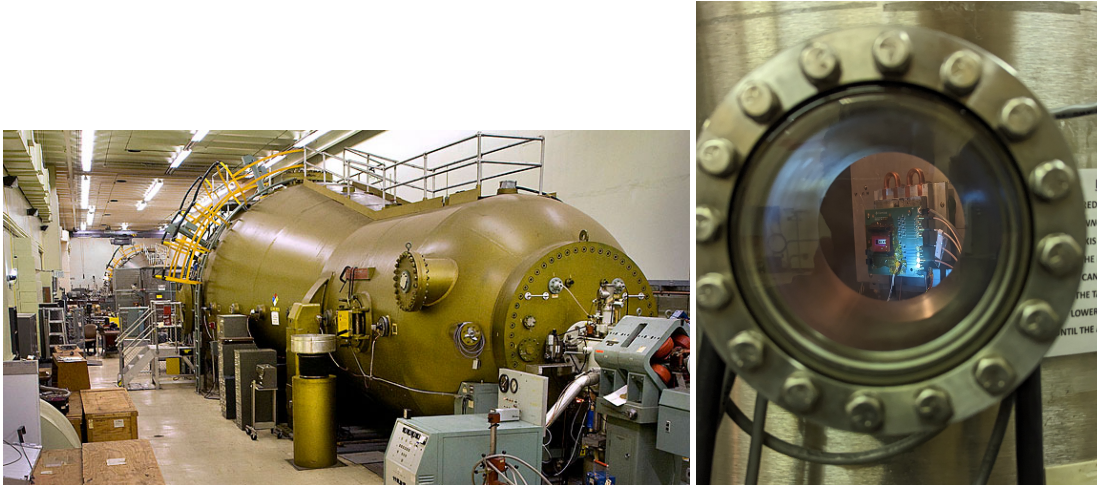


Figure 2: The tandem Van de Graaff (left) and the devices under test inside the vacuum chamber (right).

The noise level in each electronic channel (one channel corresponding to one sensor) was initially measured without beam. The average baseline noise level was confirmed with beam on an event-by-event basis as the mean of the voltage in the readout time-window prior to the signal pulse. The baseline noise was subtracted on an event-by-event basis from the measured pulse. The

standard deviation of the noise was found to be in the range 1.12 - 1.33 mV independently of the bias voltage. The trigger levels in the oscilloscope were adjusted according to the noise level in each channel and the oscilloscope voltage scale and were set in the range 5.1σ to 19.1σ above the noise. Pulses with amplitudes above 1.2 V or above the oscilloscope voltage range were rejected as they saturate the readout electronics. This selection affected only the LGAD and rejected a small fraction of events, with no significant impact on the selected data set. Events recorded by the oscilloscope were rejected if they were compatible with pick-up noise in the readout electronics.

3.3 Signal pulses in data

Examples of typical pulses from the LGAD, recorded using both 28-MeV protons and beta-particles, and those from Diode-1 for 28-MeV protons, are shown in Figure 3. As explained in the previous section, for diodes, pulses from beta-particles are not shown as the signal is small with respect to the electronic noise, and small-amplitude signals are rejected by the trigger threshold set on the oscilloscope, creating a bias on the selected pulses. To measure the signal amplitudes in diodes with MIPs, a different method is followed, see Section 5.1.2. For the LGAD, pulses are shown in Figure 3 for the bias voltage set in the range 50–225 V. For the diode, only pulses for bias voltages up to 150 V are shown. In the diode, the pulses show a small dependence on the bias voltage and do not change significantly above 150 V. In the LGAD case, the signal amplitudes are one order of magnitude greater than those in the diodes, and the increase in amplitudes as the bias voltage increases is noticeable. In addition, with a 28-MeV proton beam, the LGAD amplitude is greater than that from beta-particles by up to a factor of 8 (at 150 V bias voltage).

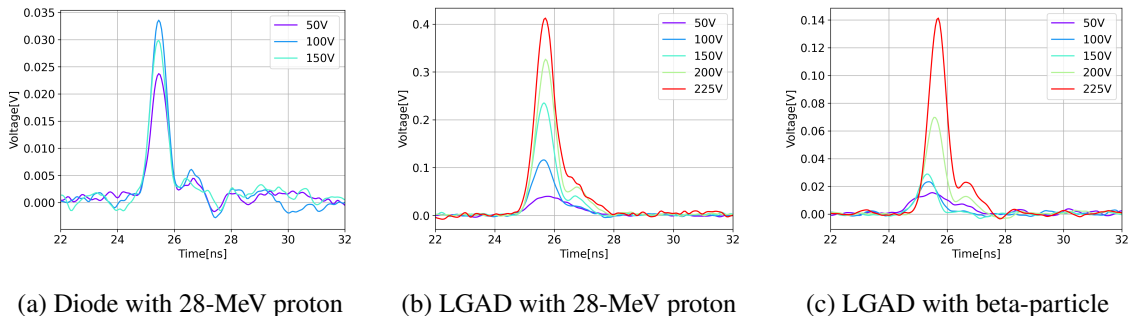


Figure 3: Examples of typical pulses generated by Diode-1 in a beam of 28-MeV protons (a), and by the LGAD in a beam of 28-MeV protons (b) and beta-particles (c) at different values of bias voltage.

4 Signal properties

To characterize the response of the LGAD to non-MIP interactions from 28-MeV protons, several key parameters are studied, such as the pulse amplitude, pulse area (the integral of the pulse as a function of time), the full-width at half-maximum (FWHM), and the rise time. The latter parameter is defined as the difference between the times when the pulse surpasses 40% and 90% of its peak value. Such threshold values were optimized to minimize the effect of noise in the rise time

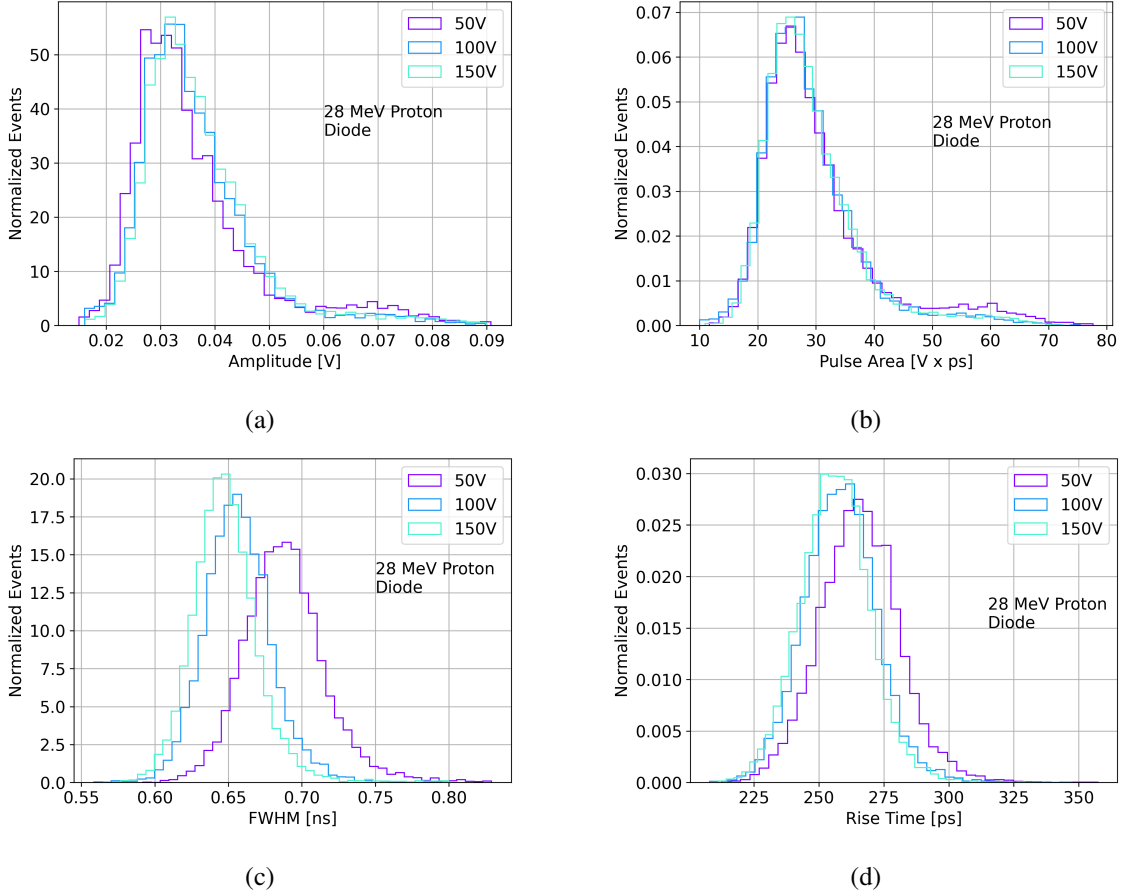


Figure 4: Area-normalized distributions of amplitude (a), area (b), FWHM (c) and rise time (d) for Diode-1 in a beam of 28-MeV protons as functions of bias voltage.

measurement. These quantities are compared to those measured with beta-particles in LGADs as well as those measured with 28-MeV protons in diodes.

4.1 Signal properties in diodes

Figure 4 shows amplitude, area, FWHM, and rise time as functions of bias voltage for Diode-1 exposed to a 28-MeV proton beam. The amplitude distribution increases little as the bias voltage increases, whereas the FWHM and rise time distributions show significant dependence on the bias voltage: the pulses become narrower and faster as the bias voltage increases.

4.2 Signal properties in LGADs

Unlike the diodes, the LGAD shows strong dependence of pulse amplitude, area, FWHM, and rise time on bias voltage. Figure 5 shows the amplitude distributions in the LGAD when it is exposed to 28-MeV protons and beta-particles at different bias voltages. For both particle beams the amplitudes increase with increasing values of the bias voltage. The amplitudes are larger in a 28-MeV proton beam than in a beta-particle beam. At a bias voltage of 225 V, the most probable value of the amplitude distribution reaches 67 mV with beta-particles and 328 mV with 28-MeV protons.

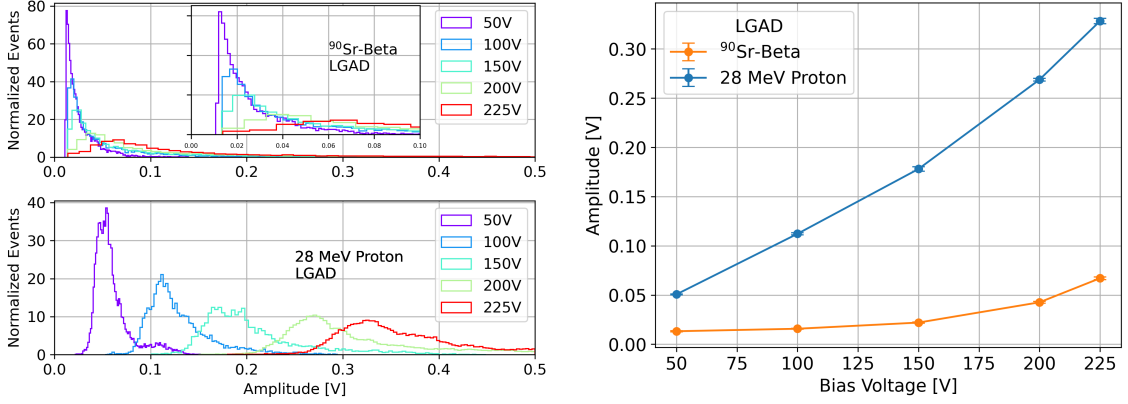


Figure 5: Area-normalized distributions of amplitudes (left) as functions of bias voltage in the LGAD, for beta-particles (left-top) and 28-MeV protons (left-bottom). Most probable values of amplitudes (right) as functions of bias voltage with beta-particles and 28-MeV protons, for the LGAD. The most probable values and their uncertainties are extracted from Gaussian fits in limited ranges around the peaks of the distributions shown on the left.

A double peaked structure was observed in the LGAD amplitude distributions; a smaller bump at low amplitudes, compatible with the amplitudes observed in diodes, was seen in addition to the main peak. This is an effect of the limited area of the gain layer with respect to the whole sensitive area, which includes the junction termination extensions and guard-rings: particles that impinge upon the LGAD at the edges of the sensitive area, outside the p^+ layer, are not multiplied, and deformations in the electric fields make them drift towards and be collected by the edge of the pad, where the electric field is low, i.e. there is no gain. Such events are removed from the event sample for further analysis by analyzing the distribution of the amplitude as a function of the FWHM, which shows a clear demarcation region between the two sets of events.

The distributions of pulse areas in the LGAD, shown in Figure 6, have a trend very similar to that of the distribution of amplitudes for both beam types, as a function of the bias voltage.

At low bias voltage, i.e. at 50 V, the LGAD pulse is very broad for both beam types, with a FWHM of about 1.5-1.9 ns, see Figure 7. The pulses become narrower when the LGAD is biased from 100 V upwards, reaching a FWHM as small as about 700-750 ps with beta-particles. The LGAD shows very similar values of FWHM with beta-particles and 28-MeV protons.

The rise times in Figure 8 show that the LGAD signal becomes faster as the bias voltage increases. More specifically, the peak of the rise time distribution decreases from about 340 ps at a bias voltage of 50 V to about 280 ps at a bias voltage of 225 V, for a beta-particle beam. The rise time distributions are very similar between the two beam types at each value of bias voltage for the LGAD.

5 Gain Measurements

The gain is measured for the LGAD using two different methods. The gain is measured as the ratio of the most probable signal amplitudes (first method) or collected charges (second method) in

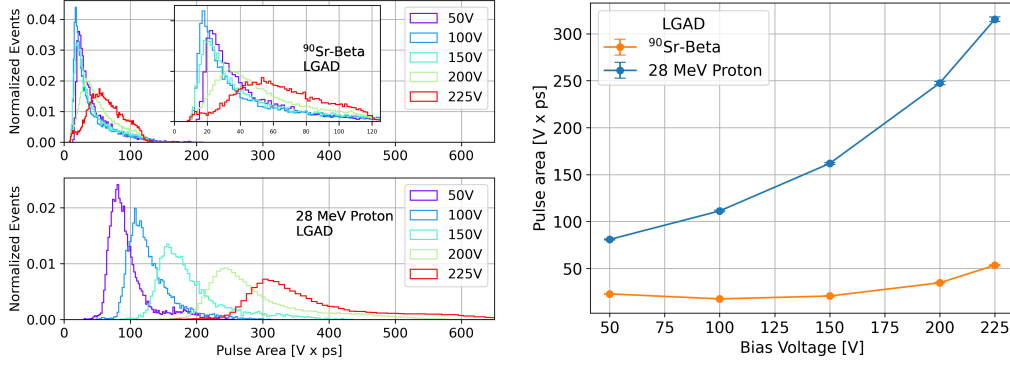


Figure 6: Area-normalized distributions of pulse area (left) as functions of bias voltage in the LGAD, for a beam of beta-particles (left-top) and 28-MeV protons (left-bottom). Mean values of pulse areas (right) as functions of bias voltage with beta-particle and 28-MeV proton beams for the LGAD. The mean values and their uncertainties are extracted from Gaussian fits in limited ranges around the peaks of the distributions shown on the left.

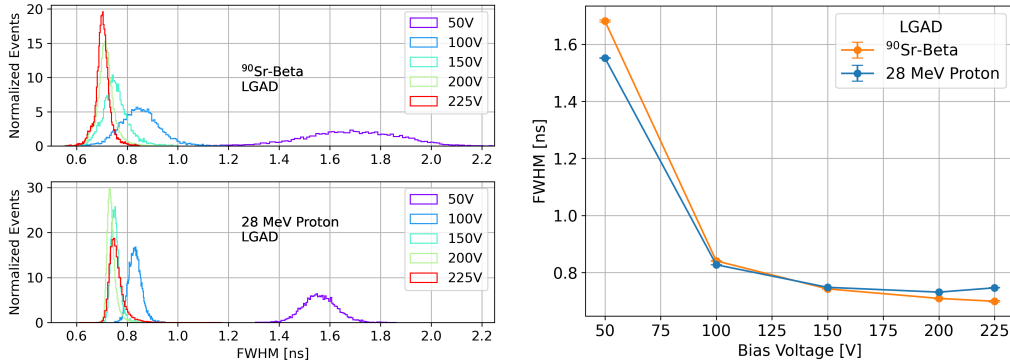


Figure 7: Area-normalized distributions of FWHM (left) as functions of bias voltage in the LGAD, for a beam of beta-particles (left-top) and 28-MeV protons (left-bottom). Mean values of FWHM (right) as functions of bias voltage with beta-particle and 28-MeV proton beams, for the LGAD. The mean values and their uncertainties are extracted from Gaussian fits in limited ranges around the peaks of the distributions shown on the left.

the LGAD and a diode under the same experimental conditions. Since different assumptions and experimental techniques are used in both methods, both sets of results are presented.

5.1 Gain from signal amplitudes

In this method the most probable values of the amplitudes are extracted for the LGAD in both beam types and for diodes in the 28-MeV proton beam from a Gaussian fit in a restricted range of the amplitude distribution around the peak. The fit range was chosen to minimize the $\chi^2/\text{n.d.f.}$ and was not greater than the full width at half maximum of the amplitude distribution. The fits result in $\chi^2/\text{n.d.f.}$ values typically ≤ 1 with the exception of about four amplitude distributions for the case

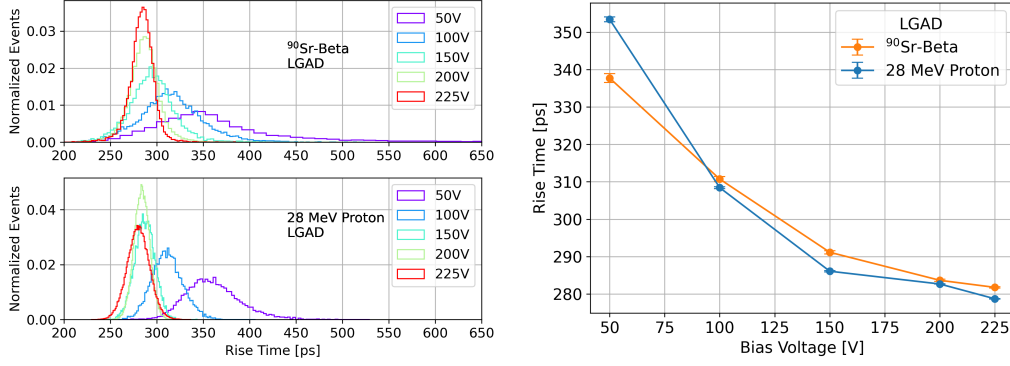


Figure 8: Area-normalized distributions of rise time (left) as functions of bias voltage in the LGAD, for a beam of beta-particles (left-top) and 28-MeV protons (left-bottom). Mean values of rise time (right) as functions of bias voltage with beta-particle and 28-MeV proton beams for the LGAD. The mean values and their uncertainties are extracted from Gaussian fits in limited ranges around the peaks of the distributions shown on the left.

of beta-particle beams, which have values between 1 and 5. For the few cases in which the $\chi^2/\text{n.d.f.}$ significantly exceeded 1, the uncertainties were adjusted to reflect the poor fit quality.

5.1.1 Gain with 28-MeV protons

In the 28-MeV proton beam, the gain is measured as the ratio of the most probable signal amplitude in the LGAD, as numerator, and the most probable signal amplitude in a diode, as denominator. The gain is measured as a function of the bias voltage for the LGAD and a diode up to 150 V. For bias voltages above 150 V, the amplitudes in the diode are taken as the values measured at 150 V, while those in the LGAD are taken at the corresponding voltage, i.e. 200 V and 225 V. The gain is measured as the average of the two gains obtained with the two diodes as denominators. The relative uncertainties from the fits of the amplitude distributions for the LGAD and diodes are included in the gain measurements. Figure 9 shows the dependence of the gain of the LGAD on the bias voltage. The gain of the LGAD ranges from about 1.6 at 50 V to 10 at 225 V.

5.1.2 Gain with beta-particles

Since the most probable value of the amplitude distribution cannot be accurately measured with beta-particles in diodes, it is extrapolated using the following method.

The measured collected charge in a diode with a MIP as incident particle corresponds to the integral of a pulse (Area) and can be expressed as follows:

$$\text{Area} = \int dt V = Q R A^2. \quad (5.1)$$

Here V is the signal voltage sampled in a time range dt ; Q is the charge generated in $35\ \mu\text{m}$ thick silicon, which is computed using 62.9 ± 3.8 as the number of electron-hole pairs generated per micron by a MIP (see Appendix A); R is the amplifier resistance, $50\ \Omega$; and A is the amplifier gain in the FNAL board, which is measured to be 9.95 ± 0.02 , using data collected with a beam of

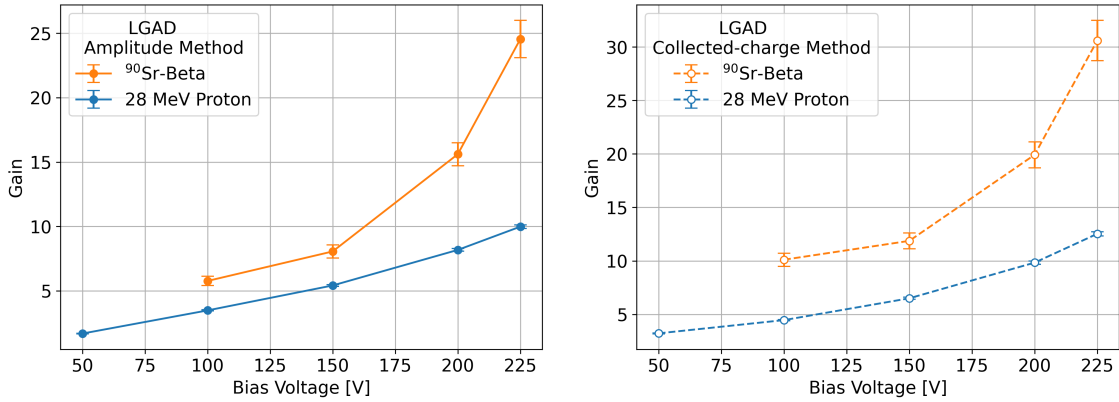


Figure 9: Gain of the LGAD as a function of bias voltage in a 28-MeV proton beam and with beta particles, using the amplitude method (Left) and the collected-charge method (Right). The data points at 50 V bias voltage are not shown for the beta-particle beam, because the associated pulse amplitudes and areas in data are truncated due to the triggering threshold in the oscilloscope (see Figures 5, 6).

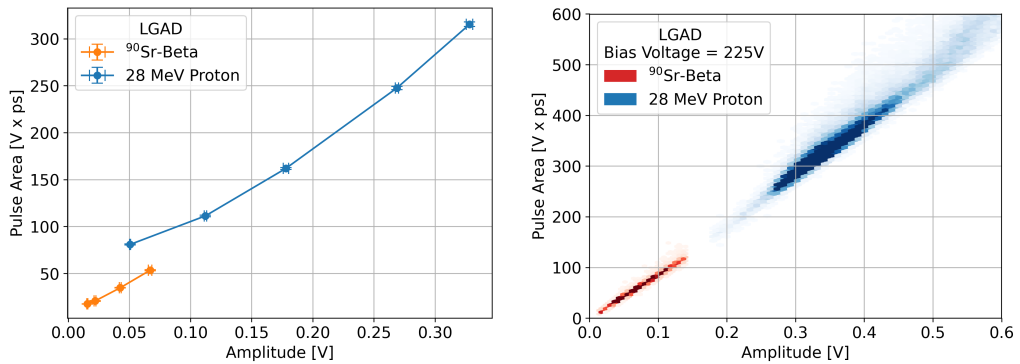


Figure 10: (Left) Mean values of the pulse area as a function of the mean values of the pulse amplitude of the LGAD in a 28-MeV proton beam and with beta-particles at the five considered bias voltages, i.e. 100, 150, 200 and 225 V. The data points at 50 V bias voltage are not shown for the beta-particle beams, because the associated pulse amplitudes and areas in data are truncated due to the triggering threshold in the oscilloscope (see Figures 5, 6). (Right) Areas as a function of amplitudes measured on a pulse-by-pulse basis for the samples collected at a bias voltage of 225 V for both beam types.

X-rays from an ^{241}Am source (see Appendix B). Thus, the value of the Area for a MIP is calculated to be (1.75 ± 0.11) V ps. The Area was experimentally observed to be linearly proportional to the amplitude, as shown in Figure 10. Thus, the most probable value of the amplitude for a MIP is obtained by extrapolating a linear fit to data from beta-particles in the two-dimensional area-amplitude distribution to the Area value of (1.75 ± 0.11) V ps (as calculated above). This results in an amplitude of (2.73 ± 0.15) mV for a diode biased at 100 V. A compatible value is found at higher bias voltages.

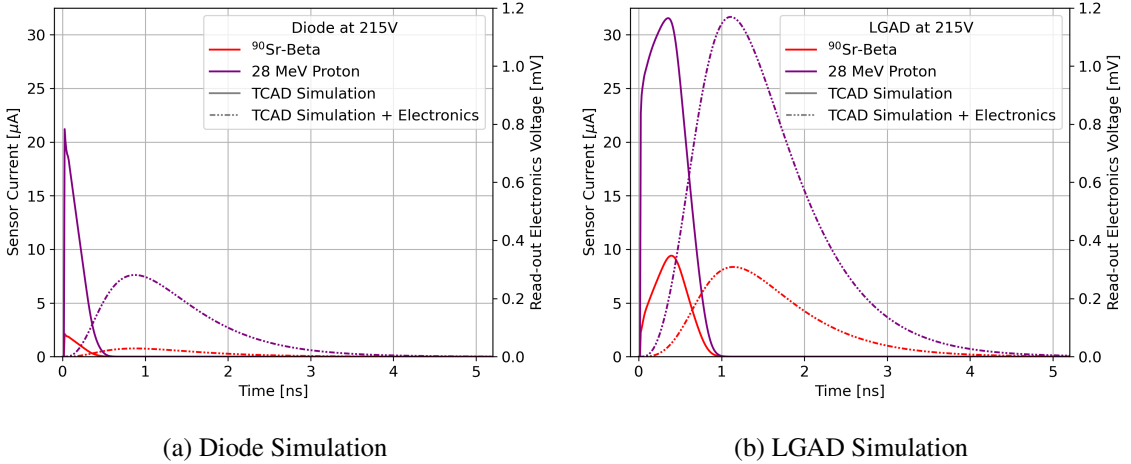


Figure 11: TCAD simulation and effect of electronics on simulation for pulses generated in a diode (left) and an LGAD (right) by a 28-MeV proton and a beta-particle from a ^{90}Sr radioactive source. In all cases, the bias voltage is set to 215 V.

The uncertainty on the gain includes the quadrature sum of the relative uncertainty on gain of the electronic board and that on the measured number of electron-hole pairs generated in a micron in silicon. The total uncertainty is dominated by those on the linear fit parameters. Systematic variations of the parametric function used in the fit, i.e. polynomial of different degrees and exponential, have a negligible impact on the diode's amplitude uncertainty: the uncertainty of the linear fit is 5.45% while the largest difference between linear fit and other parametrization is 0.02%.

Figure 9 shows that the gains with the amplitude method in a beam of beta-particles are in the approximately 5-25 range for bias voltages in the 100-225 V range, and they increase as the bias voltage increases.

5.2 Gain from collected charge

In this method the collected charges are measured for the LGAD in both beam types and for diodes in the 28-MeV proton beam by using the signal pulse area. The distributions of the pulse areas are then fit using a Gaussian function in a limited range that was chosen to minimize the $\chi^2/\text{n.d.f.}$ and was not greater than the full width at half maximum of the distribution. The fits result in $\chi^2/\text{n.d.f.}$ values generally ≤ 1 .

5.2.1 Gain with 28-MeV protons

The procedure for the measurement of the gain with 28-MeV protons using the collected-charge method is similar to the one explained in Section 5.1.1 for the amplitude method. In this method, the gain is measured as the ratio of the most probable pulse area value in the LGAD, as numerator, and the most probable pulse area value in a diode, as denominator. Figure 9 shows the gain for the LGAD as a function of the bias voltage. The uncertainties are estimated using the same method as in Section 5.1.1. In this method the LGAD gains are in the range approximately 3-13.

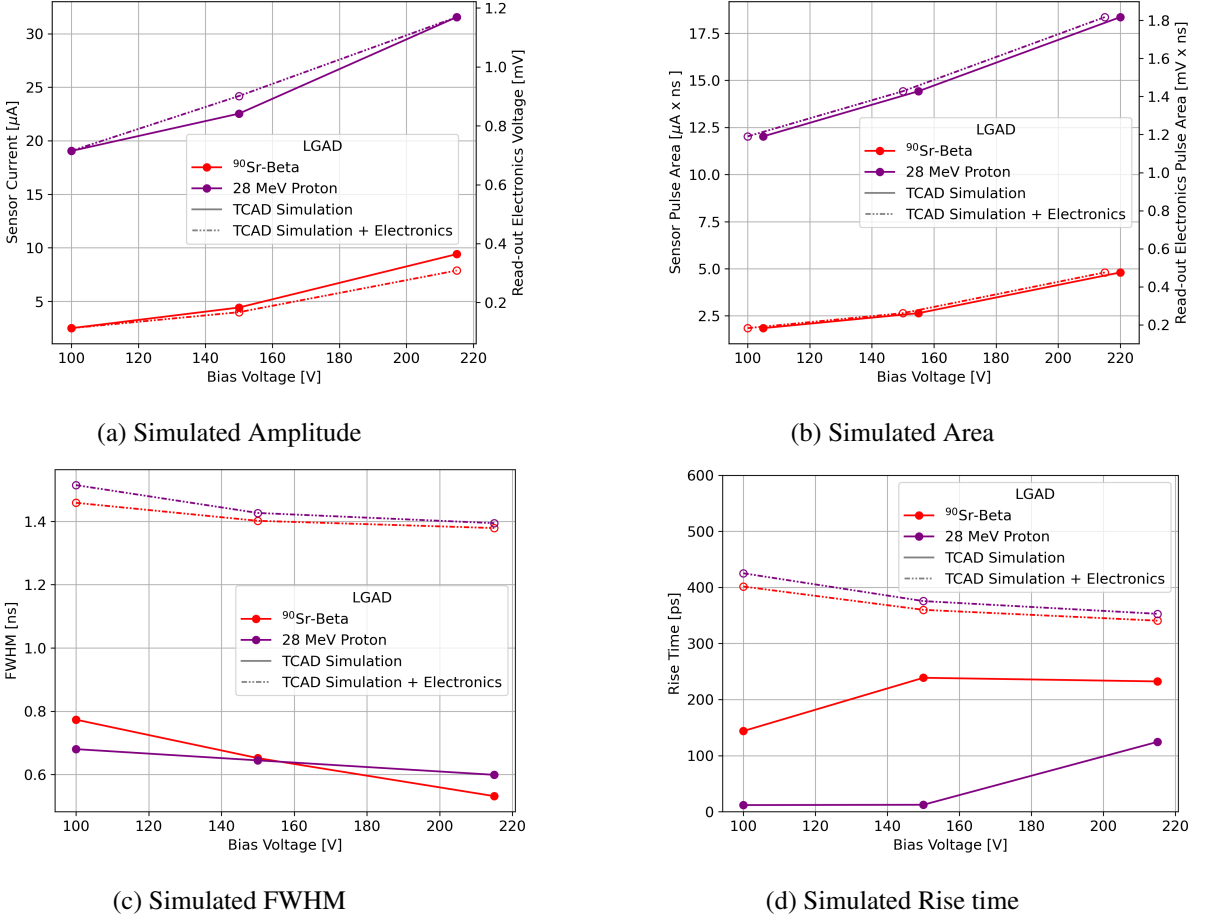


Figure 12: Simulated amplitude (a), area (b), FWHM (c) and rise time (d) in beta-particles and 28-MeV protons as functions of bias voltage, for an LGAD, with and without the effect of the readout electronics. In (b) the lines for the TCAD simulation and the one including the effect of the electronics are very close, therefore the markers of the former have been slightly shifted along the x -axis for display purposes.

5.2.2 Gain with beta particles

For the estimate of the collected charge in a diode with a beta-particle beam, the same calculations as are described in Section 5.1.2 are used. Thus, a pulse area value of 1.75 V ps is used for a MIP as the denominator in the gain calculation. Figure 9 shows the dependence of the gain as a function of the bias voltage.

6 Simulation

A SILVACO TCAD simulation was performed to predict the signal characteristics of a diode and an LGAD when they are exposed to beams of beta particles and 28-MeV protons. The geometrical characteristics and doping profiles of the sensors in simulation are qualitatively close to those of

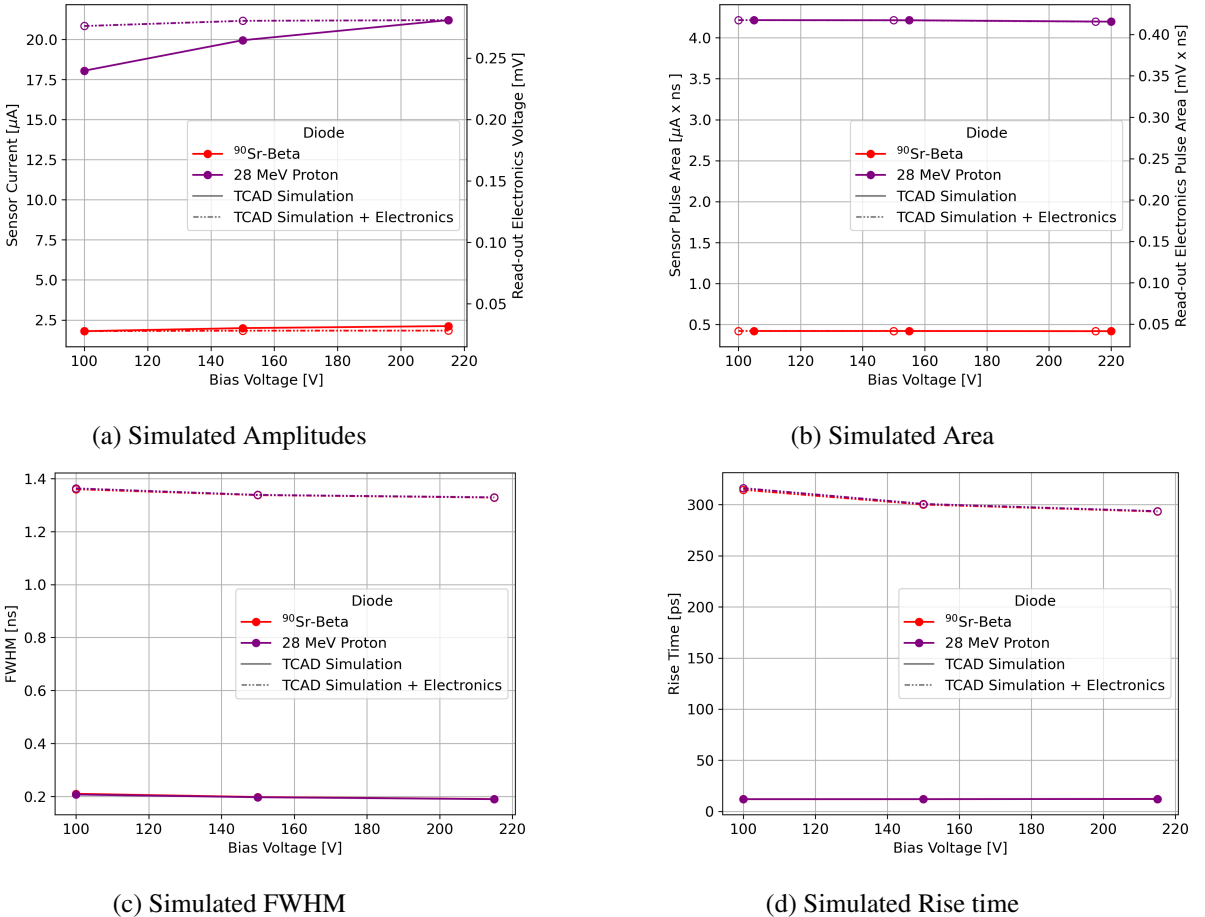


Figure 13: Simulated amplitude (a), area (b), FWHM (c) and rise time (d) in beta-particles and 28-MeV protons as functions of bias voltage, for a diode with and without the effect of the readout electronics. In (b) the lines for the TCAD simulation and the one including the effect of the electronics overlap and the markers of the former have been slightly shifted along the x -axis for display purposes. In (c) and (d) the lines for the beta-particle beam and the 28-MeV proton beam overlap.

the devices under test. The simulation was carried out for the diode and the LGAD with the bias voltages set at 100, 150 and 215 V.

Figure 11 shows the predicted pulses for a diode and an LGAD as generated by the two different particle beams when the sensors are biased at 215 V. In Table 1, the amplitude, the pulse area, the FWHM and the rise times for the LGAD and the diode are extracted from the generated pulses with the bias voltage set at 215 V. The effects of the electronics on pulses are simulated using a first-order low-pass filter response function for the two amplification stages of the readout board and the one of the oscilloscope, using the readout board and oscilloscope parameters presented in Section 2.¹

¹For simulating the two amplification stages of the readout board and the one of the oscilloscope, a transfer function of the circuit of the form $H(s) = 1/(\tau s + 1)$ was used in both cases, where s represents the Laplace variable $s = j\omega$ (with ω being the radian frequency of the sinusoidal signal) and τ represents the circuit time constant. For the amplification

Figures 12 and 13 show the values of the pulse amplitude, area, FWHM and rise time as functions of the bias voltage, simulated pre- and post-electronics for an LGAD and a diode, respectively, when impinged by a MIP and a 28-MeV proton. The effect of the electronics has a significant impact on the values of FWHM and rise time. The signals generated by the 28-MeV beam have amplitudes 10 times (diode) and about 3 times (LGAD) higher than those generated by a MIP. The values of FWHM and rise time of the LGAD and the diode are very similar in the beams of 28-MeV protons and beta-particles, when the effect of the electronics is included in the simulation. Prior to including the effect of the electronics in the LGAD signal, while the FWHM values decrease for increasing values of bias voltage, the FWHM ratios of 28-MeV protons to beta-particles increase to 1.13 at 215 V. Conversely, prior to including the effect of the electronics, the rise-time is greater in a beta-particle beam than in a 28-MeV proton beam by a factor close to 2 at 215 V. Table 1 also shows the gains of an LGAD, calculated with the two methods: as the ratio of amplitudes and of the pulse areas in the LGAD and in the diode. With both methods the simulation predicts a gain suppression close to a factor 3, in a 28-MeV proton beam compared to a MIP beam. It is also noteworthy that the two methods provide estimates of gains that differ by a factor of about 3, when the effects of the electronics are not simulated, with the area method providing the largest gain values. The difference becomes negligible when the effects of the electronics are included.

Parameter	MIP LGAD (Diode) Pre- / Post-Electronics	28-MeV Proton LGAD (Diode) Pre- / Post-Electronics
Amplitude [μA] / [mV]	9.41 (2.12) / 0.309 (0.028)	31.6 (21.2) / 1.17 (0.281)
Area [$\mu\text{A} \cdot \text{ns}$] / [mV \cdot ns]	4.80 (0.420) / 0.476 (0.0415)	18.4 (4.20) / 1.82 (0.416)
FWHM [ns]	0.532 (0.190) / 1.38 (1.33)	0.599 (0.190) / 1.39 (1.33)
Rise time [ps]	232 (12.2) / 341 (293)	124 (12.2) / 353 (294)
Gain by Amplitude Method	4.44 / 11.0	1.49 / 4.20
Gain by Area Method	11.4 / 11.4	4.37 / 4.40

Table 1: Simulation predictions for amplitude, FWHM, and rise time for a diode and an LGAD in beams of MIPs and 28-MeV protons with the sensors biased at 215 V. The LGAD gains are calculated with two methods. The parameters are reported prior to and after the simulation of the effect of the readout electronics.

7 Comparison of results

The response of the LGAD in the 28-MeV proton beam is compared to that in the ^{90}Sr -beta beam. Ratios of parameters measured in data with the 28-MeV proton beam and the ^{90}Sr -beta beam are provided as well as those predicted by the simulation.

stages, the time constant was set to $\tau = RC$, with $R = 50 \Omega$ and $C = 10 \text{ pF}$, with the latter accounting for the detector and amplifier capacitance. For the oscilloscope stage, the time constant was set to $\tau = 1/(2\pi f_c)$, with $f_c = 1 \text{ GHz}$. To simulate the total signal shaping effect, the $H(s)$ function for the two amplification stages and the oscilloscope are multiplied together with their respective τ values, while for the signal normalization, the value of the amplifier gain squared was used, i.e. $A^2 = (9.95)^2$ (see Appendix B).

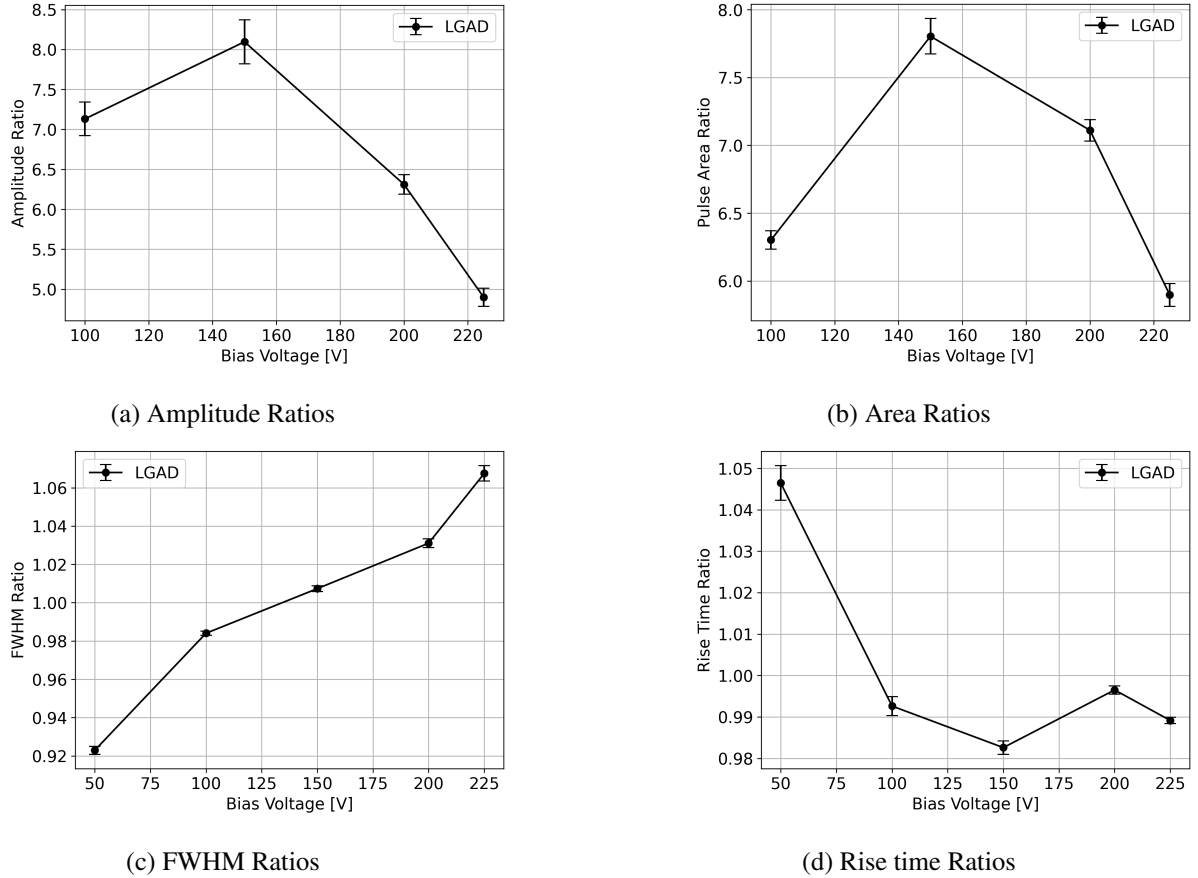


Figure 14: Ratios of amplitude (a), area (b), FWHM (c) and rise time (d) in 28-MeV protons relative to beta-particles as functions of bias voltage, for the LGAD in data. The data points at 50 V bias voltage are not shown in (a) and (b), because the associated pulse amplitudes and areas for the beta-particle beams in data are truncated due to the triggering threshold in the oscilloscope (see Figures 5, 6).

Figure 14 shows the experimental results for the ratios of amplitude, area, FWHM and rise time. The ratios of pulse amplitudes and areas are very similar. When the sensor is under a high bias voltage, i.e. at or greater than 100 V, the amplitudes and areas in a 28-MeV proton beam are in the range of 5-8 times larger than in a beta-particle beam, in agreement with the simulation that predicts the ratios to be approximately 3-8, regardless of whether the effects of the electronics are included or not. For bias voltages ≥ 100 V, the values of FWHM and rise time are stable as functions of bias voltage and very close to 1, in agreement with the simulation, with and without the effects of the electronics. Similarly, the speed of the signal (rise time) is consistent in the two beam types in data, in agreement with the simulation when the effects of the electronics are included, whereas, without the effect of the electronics, the simulation predicts it to be faster in the 28-MeV proton beam by a factor of approximately 2 at 215 V and approximately 10 or greater for lower values of bias voltage.

Strong linear correlation between the pulse amplitudes and areas is shown in Figure 10. This justifies the use of either variable for the measurement of the gain of an LGAD. The LGAD gains

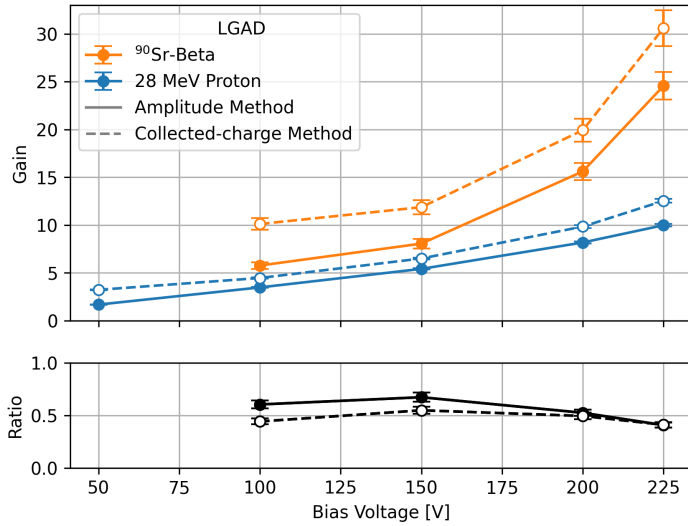


Figure 15: Gains measured using the amplitude method and the collected-charge method for the LGAD in data and in simulation as functions of bias voltage in beta-particle and 28-MeV proton beams. At the bottom the ratios of the gain in the 28-MeV proton beam to the one in the beta-particle beam are shown for each value of the bias voltage for the amplitude method and the collected-charge method. The data points at 50 V bias voltage are not shown for the beta-particle beams for the gains and in the ratios, because the associated pulse amplitudes and areas in data are truncated due to the triggering threshold in the oscilloscope (see Figures 5, 6).

measured using the two methods are compared in Figure 15 for the ^{90}Sr -beta beam and the 28-MeV proton beam. Significant systematic differences are observed between the two methods for measuring gain, with the charge-collection method giving larger gain values than the amplitude method. The difference between the gains measured with the two methods is approximately 1.5-5.0 for bias voltages greater than 100 V, for both beam types. While simulation predicts different values of gains with respect to those measured in data, it also predicts a systematic difference between the two methods for measuring the gain, but only when the effects of the electronics are not accounted for. When the effects of electronics are included in the simulation, the difference between the gains measured with the two methods is largely reduced.

Despite the systematic differences between the two methods in the measured values of gains, they both agree on the general observation of gain suppression in a 28-MeV proton beam compared to a beta-particle beam. The data show the gain suppression to be dependent on the bias voltage and to be about 2.5 with both gain-calculation methods at a bias voltage of 225 V. The simulation also predicts gain suppression of about 2.6-3.0 with both gain-calculation methods, with and without the effects of the electronics.

8 Conclusions

The performance of an LGAD was studied in a beam of 28-MeV protons and compared to that in a MIP beam from ^{90}Sr beta particles and in simulation. Pulse amplitude, width, rise time and gain, were studied as functions of the bias voltage. Qualitatively good agreement is found between data and simulation. The pulse amplitude and area are significantly larger in the 28-MeV proton beam than in the beta-particle beam, by a factor of approximately 2-8. The widths and rise time show instead smaller differences between the two particle beams. To measure the gain, two methods were used, one based on pulse amplitudes and the other on the collected charge. The two methods result in a systematic difference in the measured gains, with the one based on the collected charge yielding larger gain values in data. Despite such differences, gain suppression is observed in the LGAD with a 28-MeV proton beam with respect to a MIP beam. As for the other measured parameters, the gain suppression also depends on the bias voltage and is about 2.5 at high bias voltage. This set of results will be valuable for the use of LGAD-based sensors in non-MIP beams for applications beyond high energy or nuclear physics, such as low-energy rare processes, medical, biological, and chemical, in which beams of non-MIPs are used.

A Measurement of the number of electron-hole pairs generated by a MIP in silicon

The number of electron-hole pairs generated by a MIP in silicon was measured using a diode of $500\ \mu\text{m}$ active thickness exposed to a beam of beta-particles from a ^{90}Sr radioactive source. The sensor was read out by a charge-sensitive amplifier and the PX5 (by Amptek Inc.) readout system. The calibration of the number of readout channel counts as a function of the energy was carried out with X-rays from a ^{241}Am radioactive source. Figure 16 (left) shows the X-ray spectrum and the peak corresponding to the 59.5 keV spectrum line. The peak of the beta spectrum was found in the readout channel (channel no. 494) corresponding to 146 keV, see Figure 16 (right). Dividing this value by 3.6 eV, i.e. the energy necessary to generate an electron-hole pair in silicon, the number of electron-hole pairs generated in the $500\ \mu\text{m}$ thickness of silicon is found to be 40.6×10^3 , which corresponds to 81.20 ± 0.16 electron-hole pairs in one micron of silicon.

The number of electron-hole pairs in a silicon sensor is dependent on the thickness of the active volume [22]. The predicted value of such a parameter in the model presented in Ref. [22] (Table V) for a silicon of $500\ \mu\text{m}$ thickness was found to be compatible with the value measured experimentally and presented above. Thus, the same model was used to extrapolate 81.20 ± 0.16 for a $500\ \mu\text{m}$ thickness to 62.9 ± 3.8 for a $35\ \mu\text{m}$ thickness, where the uncertainty on the extrapolation model is conservatively increased by a factor of 5 with respect to the quoted 1.2%, because the value of the $\beta\gamma$ parameter from the beta-particle beam from the ^{90}Sr radioactive source is smaller than the one that was assumed in the model.

B Measurement of the Amplifier Gain

The amplifier gain in the FNAL board was measured using a diode fabricated by HPK with the same design as those used in the main body of this paper, mounted on the FNAL board. Data were collected with a beam of X-rays from an ^{241}Am radioactive source.

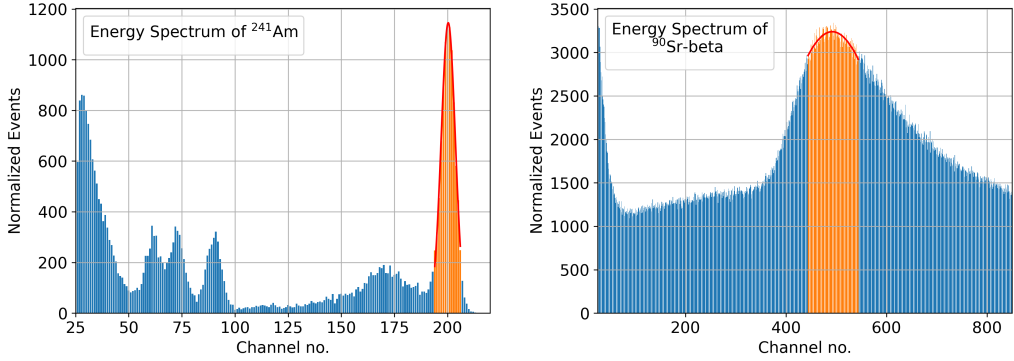


Figure 16: Energy spectra produced in a diode of $500\ \mu\text{m}$ active thickness by X-rays from an ^{241}Am radioactive source (left) and a beta-beam from a ^{90}Sr radioactive source (right). The result of the Gaussian fits around the 59.5 keV (left) and 146 keV (right) peaks are also shown, and the fit areas are colored in orange.

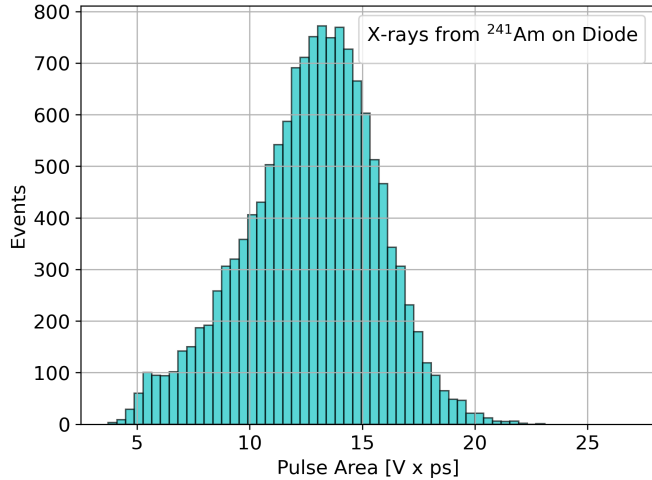


Figure 17: Distribution of the integral (area) of pulses as a function of time for ^{241}Am at 100 V, after noise rejection.

The pulse measured in an oscilloscope can be expressed as a function of the signal current as follows:

$$V_{\text{scope}} = i_{\text{signal}} \cdot (50\ \text{Ohm}) \cdot A^2, \quad (\text{B.1})$$

where A is the amplifier gain, which is squared in the above equation due to the two-stage amplification present in the FNAL board. By integrating each term in the above equation over time, we obtain the following:

$$\int dt V_{\text{scope}} = Q \cdot (50\ \text{Ohm}) \cdot A^2, \quad (\text{B.2})$$

where Q is the measured charge. From the distribution of the integral of the pulses as a function of time, as shown in Figure 17, the most probable value is measured as $\int dt V_{\text{scope}} = (12.92 \pm 0.06) \times 10^{-12} \text{ V ps}$ from a Gaussian fit to data.

The number of electron-hole pairs generated in the sensor is estimated to be 16.6 k by dividing by 3.6 eV the 59.5 keV energy of the X-ray emission from the ^{241}Am decay. The charge Q is then estimated by multiplying 16.6 k by the electron charge. Thus, the value of the amplification gain is extracted to be $A = 9.95 \pm 0.02$, in agreement with the value reported in the device data-sheet, i.e. the Mini-Circuits GALI-66+ integrated circuit [20].

As an additional cross-check, the proportionality constant between the area and the amplitude of a pulse generated by X-rays from the ^{241}Am source is compared to the one extracted in Sec. 5.1.2 for a MIP from a ^{90}Sr source, by extrapolating a linear fit to data in a two-dimensional area-amplitude distribution. For the latter, the area-to-amplitude proportionality constant is 0.66 ± 0.01 ns, while for the former the most probable values of the amplitude and area distributions are 19.0 ± 0.1 mV and 12.92×10^{-12} V ps (as reported above), respectively, leading to a proportionality constant of 0.68 ± 0.01 ns. The area-to-amplitude proportionality constant can be considered as an effective FWHM. Their values measured with X-rays and a MIP are in agreement and are also found to be compatible with the FWHM values shown in Figure 7 for an LGAD in a beta-particle beam from a ^{90}Sr source as well as for a diode in a 28-MeV proton beam, as shown in Figure 4c.

Acknowledgments

The authors wish to thank their colleagues at Brookhaven National Laboratory: Don Pinelli, Antonio Verderosa, Joe Pinz and Tim Kersten for sensor mounting. This material is based upon work supported by the U.S. Department of Energy under grants DE-SC0012704, DE-SC443363, and DE-SC426496.

References

- [1] CMS Collaboration, *A MIP Timing Detector for the CMS Phase-2 Upgrade*, Tech. Rep. [CERN-LHCC-2019-003](#). [CMS-TDR-020](#), CERN, Geneva (Mar, 2019).
- [2] ATLAS Collaboration, *Technical Proposal: A High-Granularity Timing Detector for the ATLAS Phase-II Upgrade*, Tech. Rep. [CERN-LHCC-2018-023](#). [LHCC-P-012](#), CERN, Geneva (Jun, 2018).
- [3] I. Bejar Alonso and L. Rossi, *HiLumi LHC Technical Design Report: Deliverable: D1.10*, Tech. Rep. [CERN-ACC-2015-0140](#) (Nov, 2015).
- [4] L. Rossi and O. Bruning, *High Luminosity Large Hadron Collider: A description for the European Strategy Preparatory Group*, Tech. Rep. [CERN-ATS-2012-236](#) (Aug, 2012).
- [5] H.F.W. Sadrozinski, S. Ely, V. Fadeev, Z. Galloway, J. Ngo, C. Parker et al., *Ultra-fast silicon detectors*, *Nucl. Inst. Meth. A* **730** (2013) 226.
- [6] G. Giacomini, W. Chen, F. Lanni and A. Tricoli, *Development of a technology for the fabrication of Low-Gain Avalanche Diodes at BNL*, *Nucl. Inst. Meth. A* **934** (2019) 52.
- [7] N. Moffat, R. Bates, M. Bullough, L. Flores, D. Maneuski, L. Simon et al., *Low gain avalanche detectors (LGAD) for particle physics and synchrotron applications*, *JINST* **13** (2018) C 03014.
- [8] J. Lange et al., *Gain and time resolution of 45 μm thin Low Gain Avalanche Detectors before and after irradiation up to a fluence of $10^{15} \text{ neq}/\text{cm}^2$* , *JINST* **12** (2017) P05003 [[1703.09004](#)].
- [9] Y. Zhao et al., *Comparison of 35 and 50 μm thin HPK UFSD after neutron irradiation up to $6*10^{15} \text{ neq}/\text{cm}^2$* , *Nucl. Inst. Meth. A* **924** (2019) 387 [[1803.02690](#)].
- [10] M. Li et al., *The Timing Resolution of IHEP-NDL LGAD Sensors With Different Active Layer Thicknesses*, *IEEE Trans. Nucl. Sci.* **68** (2021) 2309.
- [11] X. Yang, S. Alderweireldt, N. Atanov, M. Ayoub, J.B.G. da Costa, L.C. Garcia et al., *Layout and performance of HPK prototype LGAD sensors for the High-Granularity Timing Detector*, *Nucl. Inst. Meth. A* **980** (2020) 164379.
- [12] I. Dutta, C. Madrid, R. Heller, S. Nanda, D. Shekar, C.S. Martín et al., *Results for pixel and strip centimeter-scale AC-LGAD sensors with a 120 GeV proton beam*, *Nucl. Inst. Meth. A* **1072** (2025) 170224.
- [13] G. Giacomini, W. Chen, G. D'Amen and A. Tricoli, *Fabrication and Performance of AC-coupled LGADs*, *JINST* **14** (2019) P09004.
- [14] M. Mandurrino, R. Arcidiacono, M. Boscardin, N. Cartiglia, G.F. Dalla Betta, M. Ferrero et al., *Analysis and numerical design of Resistive AC-Coupled Silicon Detectors (RSD) for 4D particle tracking*, *Nucl. Inst. Meth. A* **959** (2020) 163479.
- [15] R. Abdul Khalek et al., *Science Requirements and Detector Concepts for the Electron-Ion Collider: EIC Yellow Report*, *Nucl. Phys. A* **1026** (2022) 122447 [[2103.05419](#)].

- [16] M. Missiaggia, E. Pierobon, M. Castelluzzo, A. Perinelli, F. Cordoni, M. Centis Vignali et al., *A Novel Hybrid Microdosimeter for Radiation Field Characterization Based on the Tissue Equivalent Proportional Counter Detector and Low Gain Avalanche Detectors Tracker: A Feasibility Study*, *Frontiers in Physics* **8** (2021) .
- [17] S.M. Mazza, *An LGAD-Based Full Active Target for the PIONEER Experiment*, *Instruments* **5** (2021) .
- [18] Brookhaven National Laboratory, *Tandem Van de Graaff*, <https://www.bnl.gov/tandem/> (2024) .
- [19] R. Heller, A. Abreu, A. Apresyan, R. Arcidiacono, N. Cartiglia, K. DiPetrillo et al., *Combined analysis of HPK 3.1 LGADs using a proton beam, beta source, and probe station towards establishing high volume quality control*, *Nucl. Inst. Meth. A* **1018** (2021) 165828.
- [20] Mini-Circuits, *GALI-S66+*, <https://www.minicircuits.com/pdfs/GALI-S66+.pdf> .
- [21] National Institute of Standards and Technology, *The PSTAR program calculates stopping power and range tables for protons in various materials*, <https://physics.nist.gov/PhysRefData/Star/Text/PSTAR.html> (2024) .
- [22] H. Bichsel, *Straggling in thin silicon detectors*, *Rev. Mod. Phys.* **60** (1988) 663.